# Single Grain Boundary Break Junction for Suspended Nanogap Electrodes with Gapwidth Down to 1–2 nm by Focused Ion Beam Milling

*Ajuan Cui, Zhe Liu, Huanli Dong, Yujin Wang, Yonggang Zhen, Wuxia Li, Junjie Li, Changzhi Gu, and Wenping Hu**

Miniaturization of electronic devices requires novel technologies to overcome the fundamental limitation of current complementary metal-oxide semiconductor (CMOS)-based technology. Devices based on carbon nanotube,[1] nanowires,[2] and nanoribbon[3] etc. have been successfully demonstrated. Building blocks based on single molecule/atom is highly expected as the ultimate limit of the minimization of electronic devices.[4] Since the properties of molecules can be tailored by molecular design, in principle, various functionalities can be obtained from designed molecules, which are beyond traditional electronic devices by elaborate choice of geometry and composition. Moreover, the lower power dissipation, higher efficiency, and ability of self-assembly and recognition make single molecular devices an ideal candidate for the next generation of electronics.[5] Indeed, molecular devices show not only properties identical or analogous to those of the diodes,[6] transistors,[7] conductors,[8] and other key components of today's microcircuits,[9] but also unique properties, which cannot find in conventional electronics.[10]

However, a great challenge for molecular devices is the connection of molecules with macroscopic electronic circuits. Comparing with top-contact junctions, devices from nanogap electrodes, with functional molecules inserted in the gap position in a planar configuration, are more prospective for future high-density integration, and have attracted a lot of attention in the past decades.[5] In addition, nanogap electrodes play an important role for fundamental investigations on mechanical, optical, and thermoelectric properties of single molecules.[11,12] Although lithography-based traditional microfabrication technologies have scaled the feature size down to tens of nanometers, its limit appears in the fabrication of sub-20 nm features in a reproducible and reliable way.[13] Several creative technologies for nanogap fabrications are developed, e.g., mechanically break junctions,[11,14] electromigrated break junctions,[15] electrochemical plating,[16] transmission electron beam (TEM) lithography,[17] selective etching,[18] and focused ion beam (FIB) lithography[19,20] and other pioneer methods such as the integration of different methods on carbon-based materials etc.[21,22] Each method has demonstrated its unique advantages for nanofabrication.[23] However, there remain some challenges encountering us, for example, using TEM or electrical measurements have shown the existence of shape instability of electromigrated break junctions.[24,25] Moreover, debris or contaminations between the electrodes and incompatibility with the existing microelectronics technology etc. also make barriers for the rapid progress of molecular devices.[26,27] Hence, new method for nanogap electrodes fabrication is needed as a potential supplementary to the existing methods to avoid such drawbacks.

Intergranular fracture is a kind of crack that takes place along grain boundaries (GBs) of a polycrystalline material, which is a phenomenon that should be usually avoided in bulk materials such as iron and various alloys as well as their thin films.[28,29] Here, we find such phenomenon could be useful for micro/nanofabrication. The intergranular fracture between two grains in a polycrystalline film can be used for the fabrication of stable nanogap electrodes with gap width down to 1–2 nm.

Some prerequisites are necessary for the fabrication of nanogap electrodes by using the phenomenon of intergranular fracture. First, for polycrystalline films, bumpy edges are always appeared after intergranular fracture, and the gap size is hard to control for the participation of multiple grains. Hence, the number of the grains along the fracture should be minimized in order to improve the controllability of operation and the morphology of the gap, and single GB is definitely the best choice. Second, single GB structure should be freestanding in order to diminish the influence of substrate in the process of intergranular fracture. Third, an extra condition is needed to trigger the occurrence of intergranular fracture on single GB junction in a relatively controllable way. Finally, the fabricated nanogap electrodes should be stable and free of debris for final using them in single molecular devices. Based on these requirements, a fabrication strategy is designed as illustrated in **Figure 1**.

Dr. A. Cui, Dr. H. Dong, Dr. Y. Zhen, Prof. W. Hu
Beijing National Laboratory for Molecular Sciences
Key Laboratory of Organic Solids
Institute of Chemistry
Chinese Academy of Sciences
Beijing 100190, China
E-mail: huwp@iccas.ac.cn
Dr. Z. Liu, Y. Wang, Dr. W. Li, Prof. J. Li, Prof. C. Gu
Beijing National Laboratory for Condensed Matter Physics
Institute of Physics
Chinese Academy of Sciences
Beijing 100190, China
Prof. W. Hu
Collaborative Innovation Center of Chemical Science and Engineering (Tianjin) & Department of Chemistry
School of Science
Tianjin University
Tianjin 300072, China

DOI: 10.1002/adma.201500527

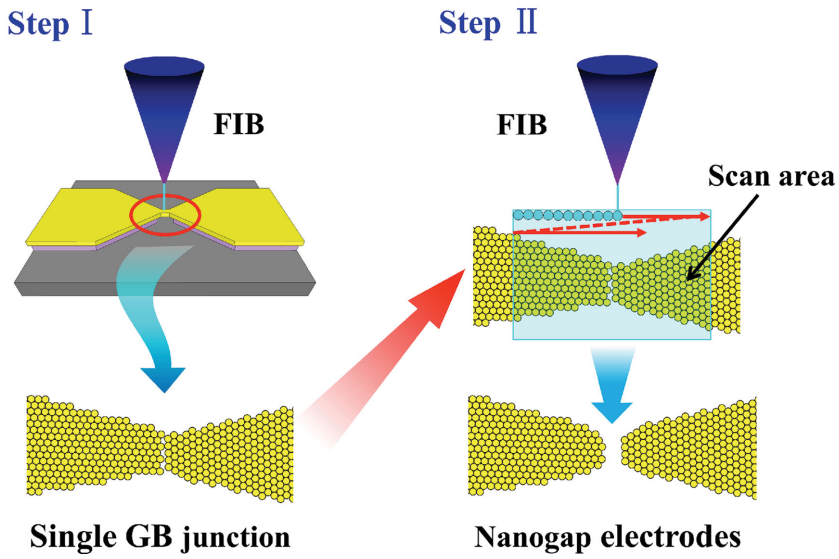


**Figure 1.** Illustration diagram of the proposed method for the fabrication of nanogap electrodes through the break of singe GB junctions: step 1, fabrication of single GB junction; step 2, break of the single GB junction by FIB milling.

The process can be divided into two key steps: the first is the fabrication of suspended single GB junction; the second is the break of the junction for nanogap electrodes. Here FIB milling is used on suspended Au wire for the formation of single GB junction and nanogap electrodes.

Heavily doped *p*-type silicon substrate with 300 nm $SiO_2$ is used as the substrate, so that it could be easily to construct single molecular transistors from the fabricated nanogap electrodes with the underlying substrate as gate electrode. Au film is deposited through a magnetron sputtering system with a thickness of 80 nm. Electron beam lithography (EBL) and reactive ion etching (RIE) are used to pattern the polycrystalline Au films into desired configuration. Then chemical etching by a hydrogen fluoride (HF) buffer solution is performed to remove the exposed $SiO_2$ layer with patterned Au film structures as mask. Due to the isotropy properties of chemical etching, the $SiO_2$ under the edge of the Au film is removed, which can be controlled by the etching time. Hence the wire, which links the two electrodes, will become suspended after the etching of the $SiO_2$. The fabrication process of suspended Au wire is illustrated in **Figure 2**a. Traditional gallium ions ($Ga^+$) FIB milling is performed on the suspended Au wire in an FIB/Scanning Electron microscope (SEM) (FEI Helios 600i) system for the fabrication of single GB junction. Reduced raster scanning strategy of FIB is used for the milling of the Au wires in a designated area. The schematic cross-section of the experiment setup is shown in Figure 2b-1, and oblique view of the experiment setup is shown in Figure 2b-2, in which FIB and the scanning path are drawn for illustration. After reduced raster scanning with FIB in a designated area, the size of the Au wire begins to decrease (Figure 2c). By controlling the ion dose during FIB milling process, the original Au wires can be milled into a bow tie-shaped structure with a neck at nanometer scale, where a single GB is always located which appeared as a dark line on the neck of the bow tie-shaped structure. The thickness of the Au film does not play a very important role except that curling of films might happen during the FIB milling process if the film is too thin or no thickness difference exists between Au film and the Au nanowire.

For the break of single GB junction, FIB milling process is adopted. The FIB milling process is similar to the fabrication of single GB junctions using an ion beam current of 7–30 pA with accelerating voltage of the ions fixed at 30 kV, taking into account of ion dose controllability, time cost, and the yield ratio of the nanogap electrodes. By performing FIB reduced raster scanning process carefully on the single GB junction, a nanogap appeared at the location of the GB, as illustrated in **Figure 3**a. For an FEI $Ga^+$ FIB system, the spot size of the ion beam is 7 nm when the beam current is fixed at 1 pA. The actual spot size is bigger for the beam current used in our experiment is 7–30 pA. Commonly, the smallest milled features are larger than the beam size of the FIB. However, gaps with size much smaller than the spot size of the ion beam are obtained in our experiment. A yield ratio of ~50% for nanogap electrodes with sub-10 nanometers gap

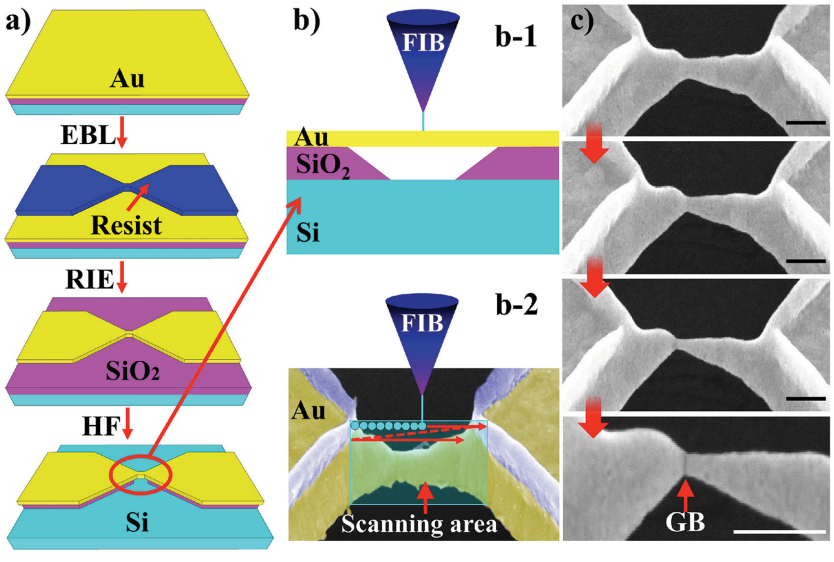


**Figure 2.** The fabrication of single GB junction: fabrication procedure and results. a) Illustration diagram of the fabrication process of suspended Au wire. b) FIB milling of suspended Au wire: schematic cross-section of the experiment setup in b-1 and illustration of the FIB scanning area and scanning path on an original suspended Au wire in b-2. c) SEM images of the same Au wire after a series of FIB milling and single GB junction was formed. The scale bar is 100 nm.

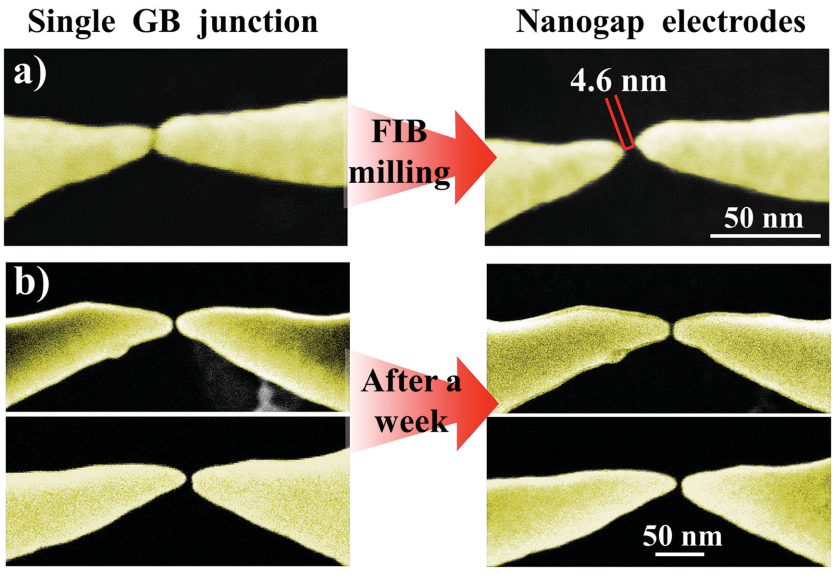


**Figure 3.** Experimental results of the nanogap electrodes fabrication through the break of single GB junction. a) SEM images of a single GB junction and that after FIB milling; b) Stability test results: the left column is the two nanogap electrodes taken right after the formation of the gap through FIB milling; the right column is that of the same structures after being kept in ambient condition for a week.

width is achieved in changing suspended nanowires (as shown in Figure 2b-2) into nanogap electrodes using an ion beam current of 7–30 pA. It should be noted that there are multiple nanogap electrodes on a single chip, and devices yield gaps below 10 nm is always over 50%, since FIB is a technique with high controllability, the yield ratio is almost the same for large number of gaps.

Nanogap electrodes are expected to be small-volume metals with large surface at the tip. For such nanoscale metal structures, the stability must be checked before its use for molecular devices. Recently, Sun et al.[30] found the shape change on a freshly fractured Ag tip under the drive of surface energy through TEM, and hence the stability of nanogap electrodes fabricated through mechanically break junction method is questionable by their observation. Same gap widening phenomenon has been reported on nanogap electrodes fabrication by electromigration.[24] Interestingly, we demonstrate that the nanogap fabrication from single GB junction is rather stable. As shown in Figure 3b, the left column is the SEM images of the as fabricated nanogap electrodes and the right column is that of the same nanogap electrodes after being kept in ambient condition for one week. No observable change in size can be found on these nanogap electrodes. The only observable difference is that deposition may occur on the Au surface during SEM imaging process a week later. Such electron-beam-induced carbonaceous deposition is caused by contamination from air or SEM chamber and can be removed by oxygen plasma or avoided by improving the storage condition.

Since characterizing the feature of the nanogap is beyond the capability of SEM, TEM is used for the observation of the nanogap. The process of the TEM sample preparation is illustrated in **Figure 4**a. After dissolving of the sacrificial layer between the Au film and the substrate, the floating Au film can be transferred onto a TEM mesh by simply taking out the mesh (the mesh is glued to another substrate for support) and Au film together with the Au film on the surface of the mesh. After dried by nitrogen, FIB is used for the formation of the suspended Au wires and the single GB junction. As can be seen from Figure 4b, a single GB always lies at the neck of the bow tie-shaped suspended wire. Figure 4c shows the TEM images of FIB milling-induced nanogap electrodes from single GB junction, both indicating that nanogap electrodes with size down to about 1 nanometers can be fabricated through the break of single GB junction. Nanogap electrodes with different size can be fabricated as shown in Figure 4c. It should be noted that the yield ratio of nanogap electrodes on the TEM mesh is not very satisfactory, which can be attributed to the stress introduced during film-transferring process and the ion beam induced bending phenomenon of the suspended Au film.

For metal films growth on insulating substrates, Volmer–Weber mode could be used to describe the initiation of film growth, which means the deposited atoms agglomerate into clusters, and then clusters grow until they impinge on each other for a continuous film. Two different grain structures can be identified due to the difference in the diffusivity of the

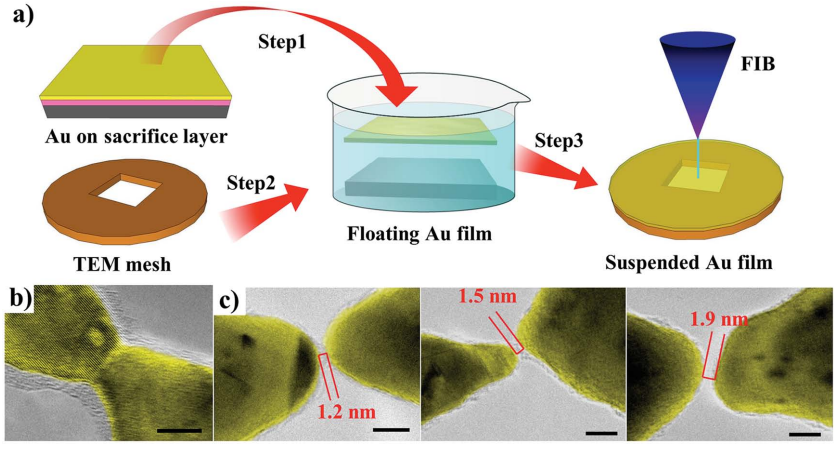


**Figure 4.** TEM characterization of the fabricated structures. a) Schematic diagram of the preparation process of suspended Au structures on TEM mesh including three steps: step 1, stripping Au film from substrate by dissolve the sacrifice layer; step 2, put the TEM mesh into the solution under the floating Au film; step 3, take out the TEM mesh with the Au film on it and dry it with $N_2$. b) TEM images of the fabricated single GB junction; c) TEM images of fabricated nanogap electrodes with 1–2 nm gap width. The scale bar is 5 nm.

material, columnar grains, or equiaxed grain structure.[31] For both structures, the GBs are almost perpendicular to the substrate plane, such GB direction is beneficial for observation of the single GB junction and nanogap. Besides, the interface will have a nearly flat configuration to minimize the total energy of the film, which is critical for the stability of the nanogap. The reason behind the instability of the Au structures reported is the big surface energy of the tip with big curvature. For our structures, the nanogap is located at the original place of the GB, which possesses a nearly flat configuration, thus minimizes the atomic migration driven by surface energy.

The mechanism behind the formation of nanogap under FIB milling can be contributed to several reasons. First, formation of nanogap electrodes at the place of the grain boundary under FIB milling manifests a preferential remove of the atoms along the grain boundary. On one hand, due to the excess free energy per unit area on the grain boundaries, the material near the grain boundaries can be removed preferentially during thermal and chemical etching processes.[32] Here, a similar effect is expected during the FIB milling process that the incident $Ga^+$ can diffuse more easily to the grain boundary, and the material composition there is changed. Similar phenomenon was reported on metal polycrystals that liquid Ga penetration can happen along grain boundaries.[33,34] Such Ga distribution along the GBs resulted in not only the change in the composition of the GB, but also decohesion between grains.[34] Such change in material composition will possibly lead to a fast milling rate under FIB. On the other hand, FIB milling process without extra precursor is a pure physical sputtering process in bulk material, and the sputtering yield is related to the parameters of both the ion beam and the target material.[35] When parameters of the ion beam scanning are fixed, the sputtering yield is determined by the incident angle of the beam to the target and the parameters of the target including atomic species, surface binding energy, and crystallographic orientation.[36] Because crystallographic orientation on the two grains of the nanogap electrodes is not necessarily the same, and the resulted gap always appears at the location of the GB, the contribution of crystallographic orientation for the formation of the nanogap electrodes could be neglected. Studies have shown that the sputtering yield of 30 keV $Ga^+$ FIB on Au increases from normal incidence at 0° to maximum sputter yield at 75°–85°.[37] For Au GB junction in Figure 3a, the sputtering rate in the GB part should be bigger than other part of the structure because of a bigger ion beam incident angle. Moreover, due to the geometry of the single GB junction, heat transfer is limited to one dimension, hence temperature raise will happen during the FIB milling process,[38] which also contributes to the preferential removing of the atoms along the grain boundary through thermal grooving phenomenon.[39] Second, FIB-induced bending of micro/nanostructures plays an important role during the nanogap formation process. For freestanding structures in micro/nanoscale, upon FIB irradiation they will intend to bent to the direction of the beam and maintain the same shape after the remove of the ion beam.[40] Such ion beam-induced bending effect is size dependent. For single GB junction, the thinnest part will tend to bent to the direction of the beam and the related force will drive the break of the GB junction, considering that the bond strength between grains is reduced by the diffusion of Ga along grain boundary. Third, the FIB/SEM dual-beam system contributes indirectly to the formation of the nanogap. Such dual-beam system allows us to observe the structure in situ by SEM while performing ion beam milling. Moreover, due to the big contrast between the suspended Au electrodes and the background, the resolution of SEM was greatly improved, which is very useful for controlling the size of GB and the gap.

With the multifunction of milling, deposition, and tomography and the advantage of site-specific, FIB is a very convenient technology for micro/nanofabrication especially for fundamental investigation. Electrodes from FIB technology were reported either through FIB milling or FIB-induced deposition,[19,27,41] however, due to the contamination of ions implantation, re-deposition of the sputtered materials and the halos effect during the FIB/FEB-induced deposition,[27,42] the fabricated electrodes are not suitable for single molecular devices. In our method, due to the suspension character of the structure, the $Ga^+$ ions implantation, re-deposition of the sputtered materials on the Si substrate do not affect the electrical properties between the two electrodes, which show superiority over traditional FIB technologies not only in fabrication precision but also in the cleanliness of the nanogap electrodes. In addition, such technique allows us to fabricate multiple nanogap electrodes on a single chip, which is important in the construction of super integrated circuits from molecular device.

In summary, we have demonstrated a new method for the fabrication of stable nanogap electrodes. Single GB junctions of Au can be fabricated into nanogap electrodes with size down to 1 nanometer through the break of such junction. Such suspended nanogap electrodes have several advantages including no debris, shape stability, and a planar configuration, which are suitable for devices fabrication with two or three terminals as promising candidates for future single molecular devices.

## Acknowledgements

The authors acknowledge National Natural Science Foundation of China (51222306, 61390503, 91323304, 91222203, 91233205, 91433115), the China-Denmark Co-project (60911130231), TRR61 (NSFC-DFG Transregio Project), the Ministry of Science and Technology of China (2011CB808405, 2011CB932304, 2013CB933403, 2013CB933504), the Strategic Priority Research Program of the Chinese Academy of Sciences (XDB12030300), Beijing NOVA Programme (Z131101000413038), and Beijing Local College Innovation Team Improve Plan (IDHT20140512).

Received: February 1, 2015
Revised: March 17, 2015
Published online: April 8, 2015

[1] a) P. L. McEuen, M. S. Fuhrer, H. K. Park, *IEEE Trans. Nanotechnol.* **2002**, *1*, 78; b) A. Javey, J. Guo, D. B. Farmer, Q. Wang, D. W. Wang, R. G. Gordon, M. Lundstrom, H. J. Dai, *Nano Lett.* **2004**, *4*, 447.
[2] a) J. Xiang, W. Lu, Y. J. Hu, Y. Wu, H. Yan, C. M. Lieber, *Nature* **2006**, *441*, 489; b) J. Goldberger, A. I. Hochbaum, R. Fan, P. D. Yang, *Nano Lett.* **2006**, *6*, 973.
[3] X. R. Wang, Y. J. Ouyang, X. L. Li, H. L. Wang, J. Guo, H. J. Dai, *Phys. Rev. Lett.* **2008**, *100*, 206803.

[4] C. Joachim, J. K. Gimzewski, A. Aviram, *Nature* **2000**, *408*, 541.
[5] T. Li, W. P. Hu, D. B. Zhu, *Adv. Mater.* **2010**, *22*, 286.
[6] A. Aviram, C. Joachim, M. Pomerantz, *Chem. Phys. Lett.* **1988**, *146*, 490.
[7] a) W. J. Liang, M. P. Shores, M. Bockrath, J. R. Long, H. Park, *Nature* **2002**, *417*, 725; b) H. Park, J. Park, A. K. L. Lim, E. H. Anderson, A. P. Alivisatos, P. L. McEuen, *Nature* **2000**, *407*, 57.
[8] a) Y. Kim, T. Pietsch, A. Erbe, W. Belzig, E. Scheer, *Nano Lett.* **2011**, *11*, 3734; b) T. Dadosh, Y. Gordin, R. Krahne, I. Khivrich, D. Mahalu, V. Frydman, J. Sperling, A. Yacoby, I. Bar-Joseph, *Nature* **2005**, *436*, 1200.
[9] a) R. Q. Wang, L. Sheng, R. Shen, B. G. Wang, D. Y. Xing, *Phys. Rev. Lett.* **2010**, *105*, 057202; b) C. B. Winkelmann, N. Roch, W. Wernsdorfer, V. Bouchiat, F. Balestro, *Nat. Phys.* **2009**, *5*, 876.
[10] C. Bruot, J. Hihath, N. J. Tao, *Nat. Nanotechnol.* **2012**, *7*, 35.
[11] J. H. Tian, B. Liu, X. L. Li, Z. L. Yang, B. Ren, S. T. Wu, N. J. Tao, Z. Q. Tian, *J. Am. Chem. Soc.* **2006**, *128*, 14748.
[12] a) S. Y. Quek, M. Kamenetska, M. L. Steigerwald, H. J. Choi, S. G. Louie, M. S. Hybertsen, J. B. Neaton, L. Venkataraman, *Nat. Nanotechnol.* **2009**, *4*, 230; b) Z. Ioffe, T. Shamai, A. Ophir, G. Noy, I. Yutsis, K. Kfir, O. Cheshnovsky, Y. Selzer, *Nat. Nanotechnol.* **2008**, *3*, 727; c) D. R. Ward, D. A. Corley, J. M. Tour, D. Natelson, *Nat. Nanotechnol.* **2011**, *6*, 33.
[13] L. Sun, Y. A. Diaz-Fernandez, T. A. Gschneidtner, F. Westerlund, S. Lara-Avila, K. Moth-Poulsen, *Chem. Soc. Rev.* **2014**, *43*, 7378.
[14] a) J. Moreland, J. W. Ekin, *J. Appl. Phys.* **1985**, *58*, 3888; b) M. A. Reed, C. Zhou, C. J. Muller, T. P. Burgin, J. M. Tour, *Science* **1997**, *278*, 252.
[15] H. Park, A. K. L. Lim, A. P. Alivisatos, J. Park, P. L. McEuen, *Appl. Phys. Lett.* **1999**, *75*, 301.
[16] a) A. F. Morpurgo, C. M. Marcus, D. B. Robinson, *Appl. Phys. Lett.* **1999**, *74*, 2084; b) Y. Kashimura, H. Nakashima, K. Furukawa, K. Torimitsu, *Thin Solid Films* **2003**, *438*, 317; c) W. P. Hu, J. Jiang, H. Nakashima, Y. Luo, Y. Kashimura, K. Q. Chen, Z. Shuai, K. Furukawa, W. Lu, Y. Q. Liu, D. B. Zhu, K. Torimitsu, *Phys. Rev. Lett.* **2006**, *96*, 027801; d) W. P. Hu, H. Nakashima, K. Furukawa, Y. Kashimura, K. Ajito, K. Torimitsu, *Appl. Phys. Lett.* **2004**, *85*, 115; e) X. L. Li, H. X. He, B. Q. Xu, X. Y. Xiao, L. A. Nagahara, I. Amlani, R. Tsui, N. J. Tao, *Surf. Sci.* **2004**, *573*, 1.
[17] a) H. W. Zandbergen, R. J. H. A. van Duuren, P. F. A. Alkemade, G. Lientschnig, O. Vasquez, C. Dekker, F. D. Tichelaar, *Nano Lett.* **2005**, *5*, 549; b) M. D. Fischbein, M. Drndic, *Nano Lett.* **2007**, *7*, 1329.
[18] a) S. H. Liu, J. B. H. Tok, Z. N. Bao, *Nano Lett.* **2005**, *5*, 1071; b) S. M. Luber, F. Zhang, S. Lingitz, A. G. Hansen, F. Scheliga, E. Thorn-Csanyi, M. Bichler, M. Tornow, *Small* **2007**, *3*, 285.
[19] T. Nagase, T. Kubota, S. Mashiko, *Thin Solid Films* **2003**, *438*, 374.
[20] T. Nagase, K. Gamo, R. Ueda, T. Kubota, S. Mashiko, *J. Microlith. Microfab.* **2006**, *5*, 011006.
[21] a) S. Kubatkin, A. Danilov, M. Hjort, J. Cornil, J. L. Bredas, N. Stuhr-Hansen, P. Hedegard, T. Bjornholm, *Nature* **2003**, *425*, 698; b) T. Jain, F. Westerlund, E. Johnson, K. Moth-Poulsen, T. Bjornholm, *ACS Nano* **2009**, *3*, 828; c) K. Moth-Poulsen, T. Bjørnholm, *Nat. Nanotechnol.* **2009**, *4*, 551.
[22] a) L. Valladares, L. L. Felix, A. B. Dominguez, T. Mitrelias, F. Sfigakis, S. I. Khondaker, C. H. W. Barnes, Y. Majima, *Nanotechnology* **2010**, *21*, 445304; b) X. L. Li, S. Z. Hua, H. D. C Chopra, N. J. Tao, *Micro Nano Lett.* **2006**, *1*, 83; c) Y. Yang, Z. B. Chen, J. Y. Liu, M. Lu, D. Z. Yang, F. Z. Yang, Z. Q. Tian, *Nano Res.* **2011**, *4*, 1199; d) X. F. Guo, J. P. Small, J. E. Klare, Y. L. Wang, M. S. Purewal, I. W. Tam, B. H. Hong, R. Caldwell, L. M. Huang, S. O'Brien, J. M. Yan, R. Breslow, S. J. Wind, J. Hone, P. Kim, C. Nuckolls, *Science* **2006**, *311*, 356; e) F. Prins, A. Barreiro, J. W. Ruitenberg, J. S. Seldenthuis, N. Aliaga-Alcalde, L. M. K. Vandersypen, H. S. J. van der Zant, *Nano Lett.* **2011**, *11*, 4607; f) X. F. Guo, A. Gorodetsky, J. K. Barton, J. Hone, C. Nuckolls, *Nat. Nanotechnol.* **2008**, *3*, 163; g) X. F. Guo, A. Whalley, J. E. Klare, L. M. Huang, S. O'Brien, C. Nuckolls, *Nano Lett.* **2007**, *7*, 1119; h) C. C. Jia, X. F. Guo, *Chem. Soc. Rev.* **2013**, *42*. 5642; i) X. F. Guo, *Adv. Mater.* **2013**, *25*, 3397.
[23] a) M. L. Perrin, R. Frisenda, M. Koole, J. S. Seldenthuis, J. A. C. Gil, H. Valkenier, J. C. Hummelen, N. Renaud, F. C. Grozema, J. M. Thijssen, D. Dulic, H. S. J. van der Zant, *Nat. Nanotechnol.* **2014**, *9*, 830; b) C. A. Martin, R. H. M. Smit, H. S. J. van der Zant, J. M. van Ruitenbeek, *Nano Lett.* **2009**, *9*, 2940; c) D. Xiang, H. Jeong, D. Kim, T. Lee, Y. J. Cheng, Q. L. Wang, D. Mayer, *Nano Lett.* **2013**, *13*, 2809; d) M. L. Perrin, C. J. O. Verzijl, C. A. Martin, A. J. Shaikh, R. Eelkema, J. H. van Esch, J. M. van Ruitenbeek, J. M. Thijssen, H. S. J. van der Zant, D. Dulic, *Nat. Nanotechnol.* **2013**, *8*, 282.
[24] D. R. Strachan, D. E. Smith, M. D. Fischbein, D. E. Johnston, B. S. Guiton, M. Drndic, D. A. Bonnell, A. T. Johnson, *Nano Lett.* **2006**, *6*, 441.
[25] K. O'Neill, E. A. Osorio, H. S. J. van der Zant, *Appl. Phys. Lett.* **2007**, *90*, 133109.
[26] a) B. Basnar, A. Lugstein, H. Wanzenboeck, H. Langfischer, E. Bertagnolli, E. Gornik, *J. Vac. Sci. Technol. B* **2003**, *21*, 927; b) P. Steinmann, J. M. R. Weaver, *J. Vac. Sci. Technol. B* **2004**, *22*, 3178; c) M. D. Fischbein, M. Drndic, *Appl. Phys. Lett.* **2006**, *88*, 063116.
[27] G. C. Gazzadi, E. Angeli, P. Facci, S. Frabboni, *Appl. Phys. Lett.* **2006**, *89*, 173112.
[28] E. A. Holm, *J. Am. Ceram. Soc.* **1998**, *81*, 455.
[29] a) D. Farkas, H. van Swygenhoven, P. M. Derlet, *Phys. Rev. B* **2002**, *66*, 060101; b) J. B. Liu, A. M. Nie, C. Z. Dong, P. Wang, H. T. Wang, M. S. Fu, W. Yang, *Mater. Lett.* **2011**, *65*, 2769.
[30] J. Sun, L. B. He, Y. C. Lo, T. Xu, H. C. Bi, L. T. Sun, Z. Zhang, S. X. Mao, J. Li, *Nat. Mater.* **2014**, *13*, 1007.
[31] L. B. Freund, S. Suresh, *Thin Film Materials: Stress, Defect Formation and Surface Evolution*, Cambridge University Press, Cambridge, UK **2003**.
[32] G. S. Rohrer, *J. Mater. Sci.* **2011**, *46*, 5881.
[33] W. Ludwig, E. Pereiro-Lopez, D. Bellet, *Acta. Mater.* **2005**, *53*, 151.
[34] E. Pereiro-Lopez, W. Ludwig, D. Bellet, J. Baruchel, *Nucl. Instrum. Meth. B* **2003**, *200*, 333.
[35] M. Nastasi, J. W. Mayer, J. K. Hirvonen, *Ion–Solid Interactions: Fundamentals and Applications*, Cambridge University Press, Cambridge, UK **1996**.
[36] B. W. Kempshall, S. M. Schwarz, B. I. Prenitzer, L. A. Giannuzzi, R. B. Irwin, F. A. Stevie, *J. Vac. Sci. Technol. B* **2001**, *19*, 749.
[37] A. A. Tseng, *J. Micromech. Microeng.* **2004**, *14*, 15.
[38] a) C. A. Volkert, A. M. Minor, *MRS Bull.* **2007**, *32*, 389; b) S. K. Tripathi, N. Shukla, S. Dhamodaran, V. N. Kulkarni, *Nanotechnology* **2008**, *19*205302.
[39] Y. Palizdar, D. San Martin, M. Ward, R. C. Cochrane, R. Brydson, A. J. Scott, *Mater. Charact.* **2013**, *84*, 28.
[40] a) A. J. Cui, J. C. Fenton, W. X. Li, T. H. H. Shen, Z. Liu, Q. Luo, C. Z. Gu, *Appl. Phys. Lett.* **2013**, *102*, 213112; b) K. Jun, J. Joo, J. M. Jacobson, *J. Vac. Sci. Technol. B* **2009**, *27*, 3043.
[41] T. Nagase, K. Gamo, T. Kubota, S. Mashiko, *Microelectron. Eng.* **2005**, *78–79*, 253.
[42] D. Brunel, D. Troadec, D. Hourlier, D. Deresmes, M. Zdrojek, T. Melin, *Microelectron. Eng.* **2011**, *88*, 1569.